Improved Size-Tunable Synthesis of Monodisperse Gold Nanorods through the Use of Aromatic Additives

Xingchen Ye,[†,⊥] Linghua Jin,[‡,⊥] Humeyra Caglayan,[§] Jun Chen,[‡] Guozhong Xing,[§] Chen Zheng,[‡] Vicky Doan-Nguyen,[‡] Yijin Kang,[†] Nader Engheta,[§] Cherie R. Kagan,[†,‡,§] and Christopher B. Murray[†,‡,*]

[†]Department of Chemistry, [‡]Department of Materials Science and Engineering, and [§]Department of Electrical and Systems Engineering, University of Pennsylvania, Pennsylvania 19104, United States. [⊥]These authors contributed equally to this work.

ABSTRACT

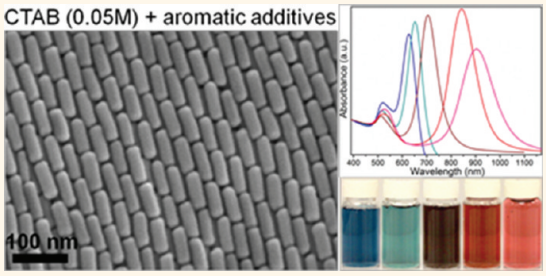

We report an improved synthesis of colloidal gold nanorods (NRs) by using aromatic additives that reduce the concentration of hexadecyltrimethylammonium bromide surfactant to ~0.05 M as opposed to 0.1 M in well-established protocols. The method optimizes the synthesis for each of the 11 additives studied, allowing a rich array of monodisperse gold NRs with longitudinal surface plasmon resonance tunable from 627 to 1246 nm to be generated. The gold NRs form large-area ordered assemblies upon slow evaporation of NR solution, exhibiting liquid crystalline ordering and several distinct local packing motifs that are dependent upon the NR's aspect ratio. Tailored synthesis of gold NRs with simultaneous improvements in monodispersity and dimensional tunability through rational introduction of additives will not only help to better understand the mechanism of seed-mediated growth of gold NRs but also advance the research on plasmonic metamaterials incorporating anisotropic metal nanostructures.

KEYWORDS: monodisperse · gold nanorods · CTAB · salicylic acid · self-assembly · superlattice · plasmonics

The field of plasmonics has been one of the most exciting and active research areas in nanoscience and nanotechnology.[1−6] The resonant excitation of surface plasmons on subwavelength metallic nanostructures provides ways to manipulate electromagnetic waves beyond the diffraction limit and to tailor light−matter interactions at the nanoscale, which may enable a rich variety of new technologies including plasmonic solar cells,[4] surface-enhanced spectroscopies,[7−10] sensing,[11−13] bioimaging and therapeutics,[14−16] drug delivery,[17,18] superlenses,[19] nanolasers,[20] optical recording,[21] and plasmonic rulers.[22]

Chemical synthesis of metal nanostructures with well-controlled size and morphology represents a versatile bottom-up approach for accessing nanoscale plasmonic building blocks.[23−25] Gold nanorods (NRs), with a broadly tunable aspect-ratio-dependent longitudinal surface plasmon resonance (LSPR), are one of the most studied colloidal plasmonic nanostructures.[26−28] Seeded growth of gold NRs in aqueous medium, pioneered by Murphy *et al.* and later improved by El-Sayed *et al.*,[29−31] has been well-documented in terms of control over NR size and shape uniformity and the spectral tunability of the LSPR. The original idea was to use micelles formed by the cationic surfactant hexadecyltrimethylammonium bromide (CTAB) as a "soft template" to direct NR formation. Since then, factors including temperature,[28] pH,[32−34] crystallinity of seed particles,[35,36] concentration of reactants,[33,37−39] single-component surfactants other than CTAB,[40,41] binary surfactant mixtures,[31,37] and the presence of iodide ions in the growth solution[42−46] have been carefully evaluated by several research groups, and many modifications of the initial recipe have been carried out to help gain a better understanding of the reaction mechanism. These efforts have led to the speculation that rather than micelle-templated growth, preferential binding of CTAB molecules onto certain facets of developing NRs seems to be operative in the growth of gold NRs.[26,27] Importantly, Murphy *et al.* and Jin *et al.* demonstrated that the high concentration of CTAB (0.1 M) needed for gold NR formation is indeed a requirement for the high concentration of bromide counterions, although in both reports, control over NR monodispersity under reduced CTAB concentration was not

* Address correspondence to cbmurray@sas.upenn.edu.

Received for review January 22, 2012 and accepted February 29, 2012.

Published online February 29, 2012
10.1021/nn300315j

found to be better than the standard procedure.[47,48] Despite these advances in gold NR synthesis and recent progress in postsynthetic shape-selective purification of NRs from nonrod-shaped byproducts,[49−51] the quality or monodispersity of the as-synthesized gold NRs (this is particularly true for NRs with a LSPR less than 700 nm or greater than 900 nm) using existing protocols is still far from ideal.

It is well-known that surfactant molecules self-assemble into micelles in aqueous solution above the critical micelle concentration.[52] Certain cationic surfactants such as alkyltrimethylammonium halide and alkylpyridinium halide can form rodlike or wormlike micelles at high concentrations, thus rendering the solution viscoelastic.[53] In particular, it has been shown that the micellization behavior of CTAB surfactant can be modified through the addition of certain aromatic compounds such as sodium salicylate.[54−57] Inspired by knowledge on the complex phase behavior of cationic surfactants in the presence of aromatic counterions from the surfactant science community and numerous efforts to elucidate the mechanism of seeded growth of gold NRs, we exploit the possibility of using those aromatic additives in combination with a reduced amount of CTAB surfactant for improved synthesis of gold NRs.

In this work, we report an improved synthesis of colloidal gold NRs through seed-mediated growth. What has been widely accepted as "essential ingredients" for gold NR synthesis such as CTAB, silver ion, ascorbic acid, and CTAB-capped gold seeds are maintained in this newly developed methodology. However, we demonstrate that through judicious choice of aromatic additives, monodisperse Au NRs with negligible shape impurities (<1% of the total number of particles) and broadly tunable LSPR peaks can be synthesized under a significantly reduced concentration of CTAB (~0.05 M) in the NR growth solution.

RESULTS AND DISCUSSION

Synthesis of Gold NRs with LSPRs Less than 700 nm Using Salicylate-Based Sodium Salts. Seed-mediated growth in the presence of the cationic surfactant CTAB has been continuously improved since its first demonstration by Murphy *et al*. and is now widely adopted for the preparation of gold NRs.[29,31] The NRs obtained typically exhibit LSPRs greater than 700 nm, corresponding to a NR aspect ratio larger than ~2.8. Preparation of gold NRs of relatively small aspect ratio has been demonstrated using mild oxidation with Au(III)−CTAB complexes,[58] O_2 or H_2O_2 in an acidic environment,[59,60] anisotropic chemical etching with cyanide or ferric chloride,[61,62] laser-induced thermal heating,[63] and controlled overgrowth of preformed gold NRs.[60,64] However, these postsynthetic modification strategies usually offer limited control over size and shape uniformity of the final products, and thus a one-step synthesis of monodisperse short gold NRs with LSPRs in the visible region is still desirable.

To grow short gold NRs, here we report the use of salicylate-based organic salts as the additive together with CTAB (~0.05 M in the growth solution) whose concentration has been reduced by 50% compared to the standard recipes (0.1 M). It has been widely accepted that the hydrophobic benzene ring of the additive tends to penetrate into the hydrophobic alkyl chain of the CTAB monomer. Meanwhile, the salicylate anion can orient in such a way that the negatively charged COO^- group stands perpendicular to the surfactant and projects radially from the surface of the micelle into the bulk aqueous solution.[54,55] These two factors change synergistically the micellar packing parameter $p = v/Al$, where v is the effective volume of the hydrophobic chain, A is the effective area of the polar headgroup, and l is the length of the hydrocarbon chain.[52] Insertion of the phenyl moiety of the salts increases the v of the CTAB micelle. Anion association reduces the micellar surface charge and decreases A by reducing the electrostatic repulsion between the quaternary ammonium groups, promoting the spherical to rodlike micellar transition. In this work, the two aromatic salt additives tested for gold NR synthesis are sodium 3-methylsalicylate and sodium salicylate. Figures 1a,b and S2 show the TEM images of gold NRs synthesized with 0.0126 M sodium 3-methylsalicylate present in the growth solution. The NRs obtained have an average diameter of 14.0 ± 1.0 nm and a length of 33.0 ± 2.5 nm (corresponding to an aspect ratio of ~2.4), giving rise to a LSPR peak centered at about 627 nm. On the other hand, slightly longer NRs are made when 0.010 M sodium salicylate is used as the additive. As shown in Figures 1d,e and S3, the NRs exhibit average dimensions of 14.0 ± 1.2 nm in diameter and 36.0 ± 2.5 nm in length (corresponding to an aspect ratio of ~2.6), resulting in a LSPR band around 653 nm. In both cases, the level of shape impurities such as spherical nanoparticles or nanoplates in as-synthesized samples is dramatically lower than those of previous gold NR preparations using silver-assisted seed-mediated growth, which is also evidenced by the strong, sharp LSPR peaks in the ensemble extinction spectra (Figure 1g). HRTEM images (Figure 1c,f) indicate that gold NRs grown in the presence of aromatic sodium salt additives are single-crystalline with a [001] growth direction. It is worth pointing out that recent crystallographic studies of gold NRs showed that the side facets of gold nanorods are dominated by high-index planes.[65,66]

Synthesis of Gold NRs with LSPRs Greater than 700 nm Using Aromatic Acid Additives. To explore the possibility of tuning the aspect ratio of gold NRs and study the effects of different aromatic additives on gold NR

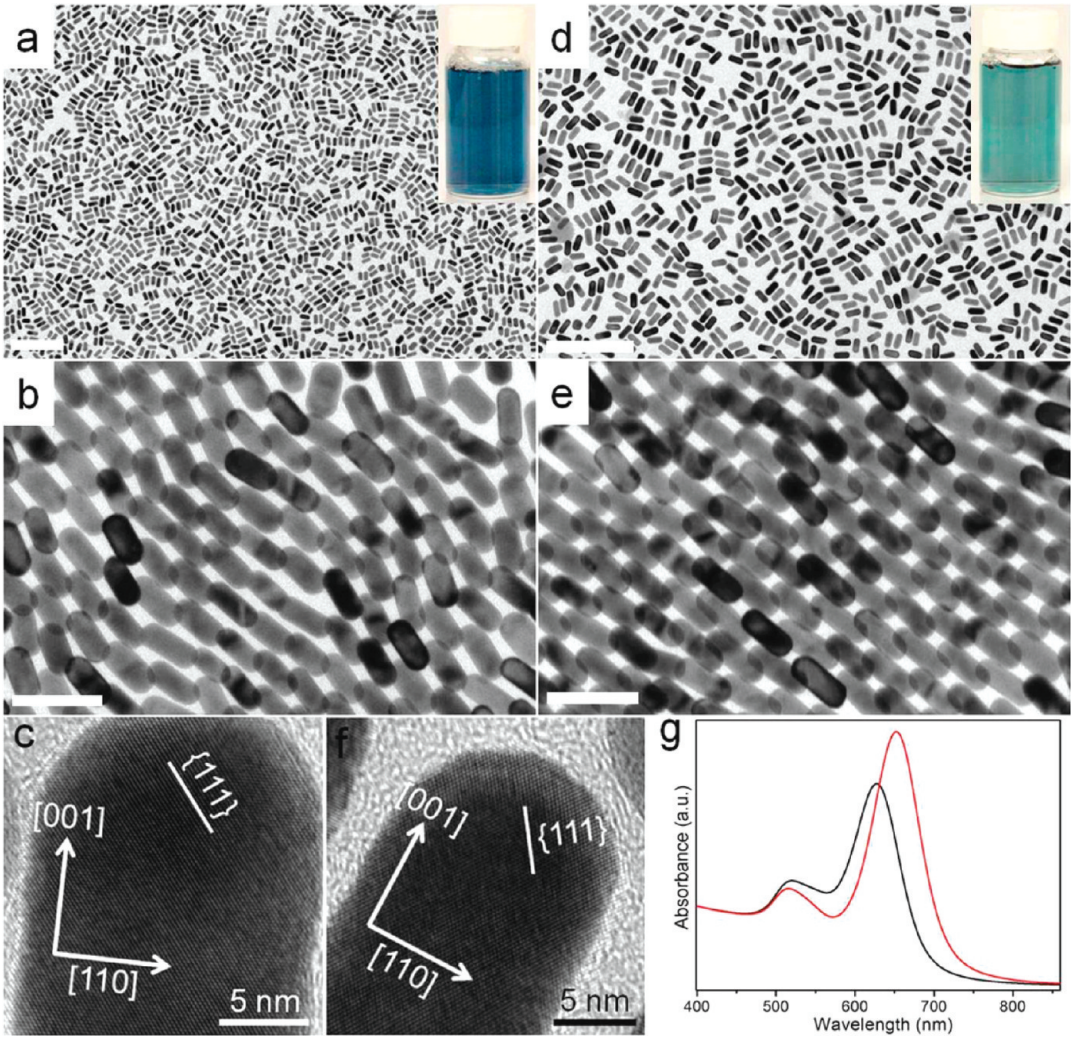

Figure 1. Synthesis of monodisperse gold NRs with LSPRs less than 700 nm using salicylate-based sodium salt additives. (a, b) TEM images and (c) HRTEM image of gold NRs synthesized under conditions specified in Table S1 using sodium 3-methylsalicylate as the additive. (d, e) TEM images and (f) HRTEM image of gold NRs synthesized under conditions specified in Table S1 using sodium salicylate as the additive. The insets of (a) and (d) show the photograph of the corresponding aqueous dispersion of gold NRs. (g) UV−vis−NIR spectra of gold NRs synthesized under conditions specified in Table S1 using additives sodium 3-methylsalicylate (black curve) and sodium salicylate (red curve), respectively. Each spectrum is normalized by its absorption at 400 nm. Scale bars: (a) 200 nm, (b) 50 nm, (d) 200 nm, (e) 50 nm.

growth, the acid forms of those aromatic additives such as salicylic acid and its common chemical variants are employed (Figure S1). The amount of each additive is optimized so that the NR growth solution is not too viscous to allow the needed solute diffusion at a CTAB concentration of ~0.05 M. As shown in Figure 2, gold NRs with negligible shape impurities are obtained by using 5-bromosalicylic acid or 2,6-dihydroxybenzoic acid as the additive, with NR dimensions of (46.0 ± 3.0 nm) × (12.0 ± 1.0 nm) and (51.5 ± 3.0 nm) × (15.5 ± 1.5 nm), respectively (Figures 2a−d, S4, S5). However, a small fraction of spherical nanoparticles does exist in the as-synthesized gold NR sample using the additive 4-methylsalicylic acid (Figures 2e,f and S6), although the dimensions ((51.0 ± 3.0 nm) × (14.0 ± 1.5 nm)) of the NRs are nearly identical to those obtained with the additive 5-bromosalicylic acid. The amount of shape impurities is also reflected by intensities of the absorption shoulder around 545 nm in the extinction spectra (Figure 2i). The narrow LSPR peaks centered at about 750 nm for additives 5-bromosalicylic acid (full width at half-maximum, fwhm = 104 nm) and 4-methylsalicylic acid (fwhm = 97 nm) and around 730 nm for additive 2,6-dihydroxybenzoic acid (fwhm = 93 nm) further confirm the monodispersity of the gold NRs. HRTEM images show that the NRs are single-crystalline, growing along the [001] direction (Figure 2g, h), similar to the shorter NRs prepared using aromatic sodium salt additives (Figure 1c,f).

Moreover, utilizing 3-methylsalicylic acid or salicylic acid (Figures S9, S10) as the additive consistently results in a larger fraction of spherical and quasi-spherical impurities in the gold NR products compared to additives 5-bromosalicylic acid or 4-methylsalicylic

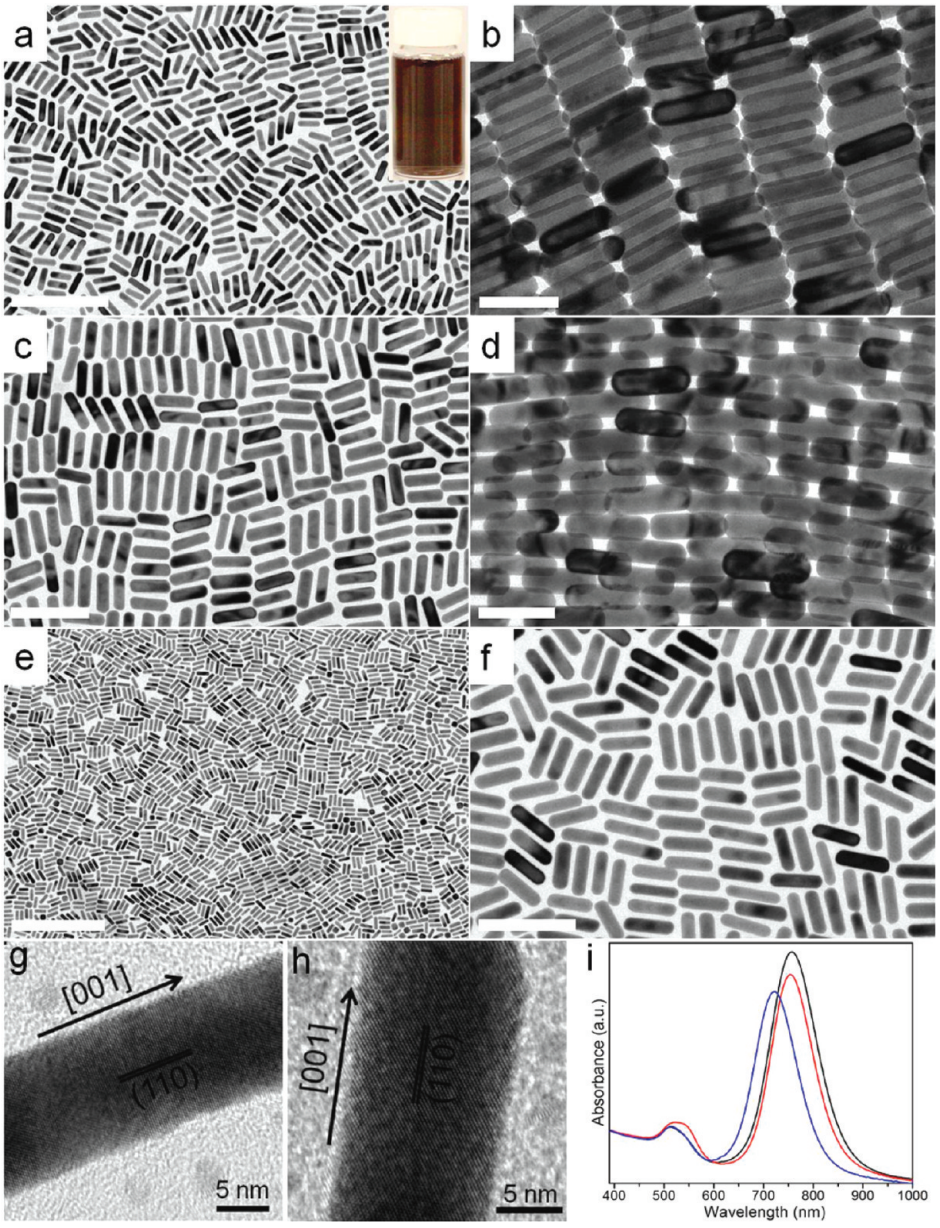

Figure 2. Synthesis of monodisperse gold NRs with LSPRs greater than 700 nm using aromatic acid additives. (a, b) TEM images and (g) HRTEM image of gold NRs synthesized under conditions specified in Table S1 using 5-bromosalicylic acid as the additive. The inset of (a) shows the photograph of the corresponding aqueous dispersion of gold NRs. (c, d) TEM images and (h) HRTEM image of gold NRs synthesized under conditions specified in Table S1 using 2,6-dihydroxybenzoic acid as the additive. (e, f) TEM images of gold NRs synthesized under conditions specified in Table S1 using 4-methylsalicylic acid as the additive. (i) UV–vis–NIR spectra of gold NRs synthesized under conditions specified in Table S1 using additives 5-bromosalicylic acid (black curve), 4-methylsalicylic acid (red curve), and 2,6-dihydroxybenzoic acid (blue curve), respectively. Each spectrum is normalized by its absorption at 400 nm. Scale bars: (a) 200 nm, (b) 50 nm, (c) 400 nm, (d) 100 nm, (e) 100 nm, (f) 50 nm.

acid, although in all four cases, the NRs formed have very similar dimensions and thus LSPR wavelength. The pH value of each NR growth solution is measured to be ~2.0 (Table S3), thus ruling out the role of pH that might account for the differences in gold NR sample quality.

Furthermore, altering the chemical nature of the functional groups on the aromatic additives also seems to have dramatic impacts on the uniformity of gold NR products. While 5-chlorosalicylic acid causes a greater percentage of shape impurities and larger size distribution of as-synthesized gold NRs in comparison to 5-bromosalicylic acid (Figure S11), 5-aminosalicylic acid leads to almost exclusively irregularly shaped nanoparticles rather than NRs, as evidenced by the disappearance of the LSPR band in the absorption spectrum (Figures S12, S13).

Fine-Tuning of Gold NR Dimensions in Certain CTAB–Aromatic Additive Systems. To grow NRs with larger aspect ratios and exploit the tunability of NR dimensions for a

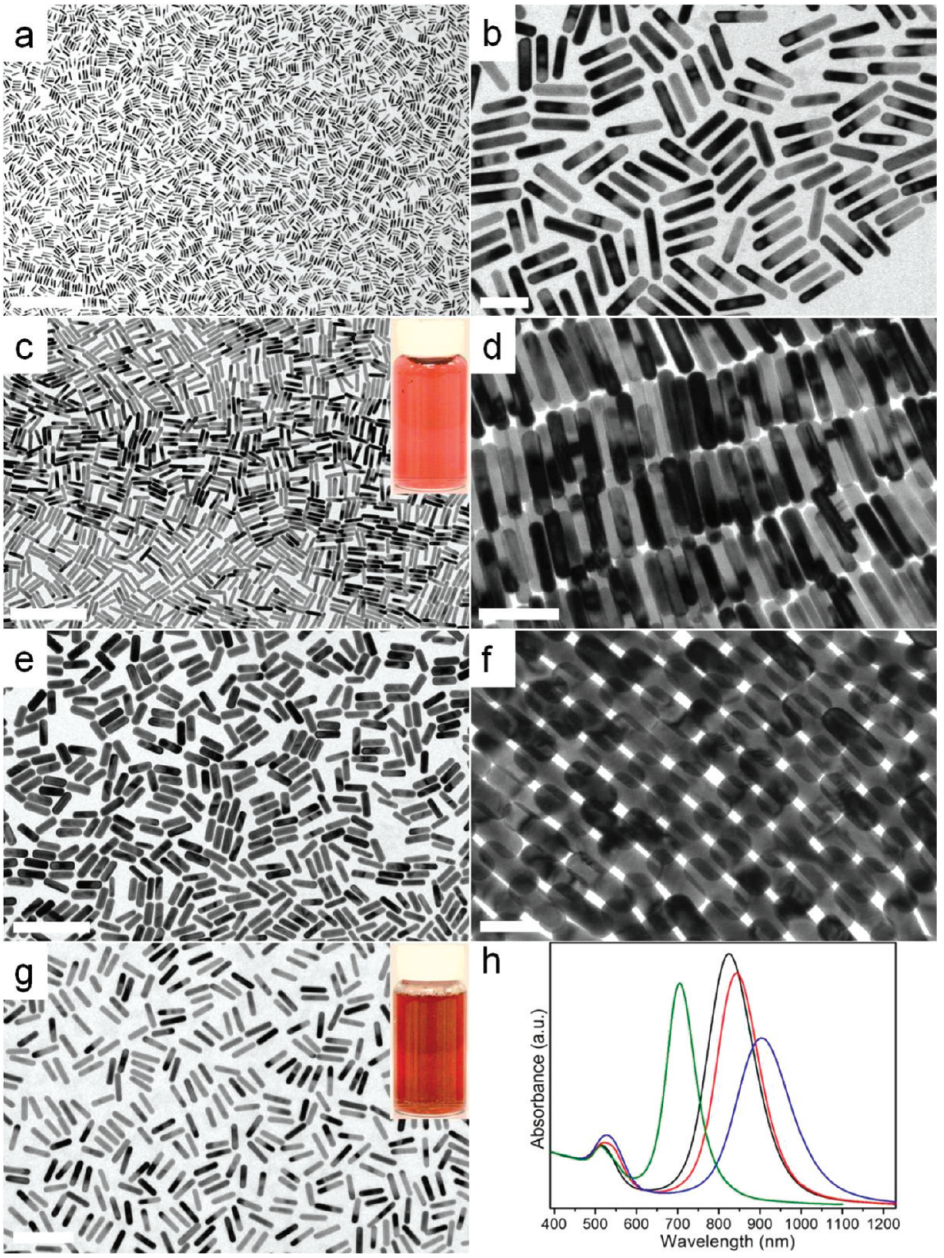

Figure 3. Fine-tuning of gold NR aspect ratio using 5-bromosalicylic acid as the additive. (a, b) TEM images of gold NRs synthesized with 0.4 mL of seed solution and 18 mL of 4 mM $AgNO_3$ solution. (c, d) TEM images of gold NRs synthesized with 0.8 mL of seed solution and 24 mL of 4 mM $AgNO_3$ solution. (e, f) TEM images of gold NRs synthesized with 0.2 mL of seed solution and 12 mL of 4 mM $AgNO_3$ solution. (g) TEM image of gold NRs synthesized with 0.4 mL of seed solution and 12 mL of 4 mM $AgNO_3$ solution. The insets of (c) and (g) show the photograph of the corresponding aqueous dispersion of gold NRs. (h) UV−vis−NIR spectra of gold NRs shown in a and b (red curve), c and d (blue curve), e and f (green curve), and g (black curve), respectively. Each spectrum is normalized by its absorption at 400 nm. Scale bars: (a) 500 nm, (b) 50 nm, (c) 200 nm, (d) 50 nm, (e) 200 nm, (f) 50 nm, (g) 100 nm.

given CTAB−aromatic additive system, silver ion content or the amount of seed solution added to the NR growth solution is systematically adjusted.[31,37,38] For the CTAB−sodium 3-methylsalicylate combination, it is found that the effect of increasing silver ion content is not to increase the aspect ratio of nanorods, but to increase the portion of spherical nanoparticles (Figure S15). However, greater dimensional control (aspect ratio from 2.9 to 4.9) and thus spectral tunability (LSPR wavelength from 705 to 904 nm) are achieved for the CTAB−5-bromosalicylic acid system (Figure 3). The general trend is the more silver ions or the fewer seed particles present in the growth solution, the longer the NRs (Table S2). Interestingly, when 0.2 mL of seed solution is used, it does induce elongation (64.0 ± 5.0 nm in length) of the NR compared to the case of 0.4 mL of seed solution (44.0 ± 3.5 in length) with identical silver ion concentration (Figure 3e−g, S19−S21), but the increase in width is more significant (*i.e.*, fatter NRs), giving rise to a smaller NR aspect ratio

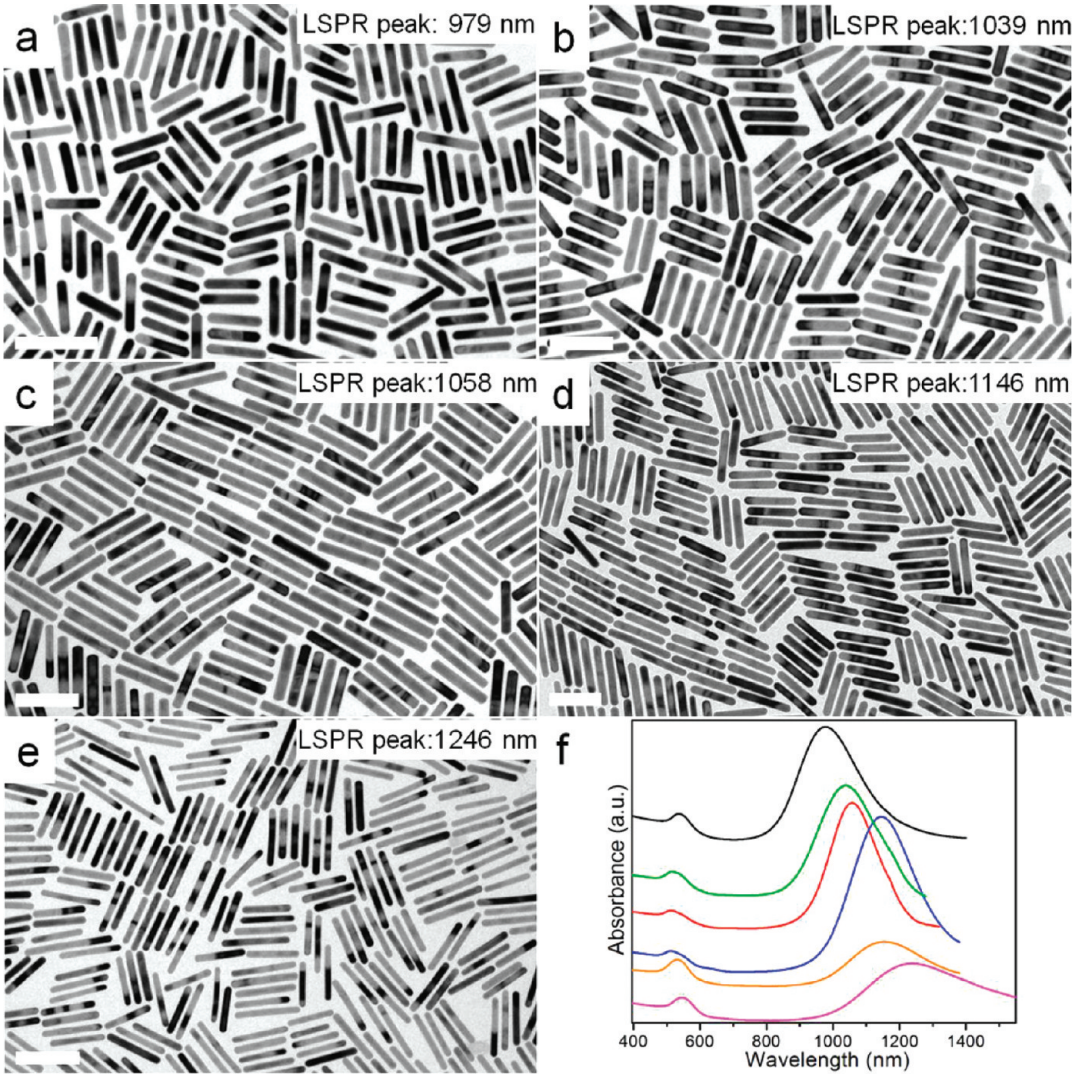

Figure 4. Synthesis of high aspect ratio gold NRs with the addition of HCl using 5-bromosalicylic acid as the additive. (a) TEM image of gold NRs synthesized with 0.8 mL of seed solution and 60 mL of 4 mM $AgNO_3$ solution. (b) TEM image of gold NRs synthesized with 0.4 mL of seed solution and 24 mL of 4 mM $AgNO_3$ solution. (c) TEM image of gold NRs synthesized with 0.4 mL of seed solution and 48 mL of 4 mM $AgNO_3$ solution. (d) TEM image of gold NRs synthesized with 0.2 mL of seed solution and 36 mL of 4 mM $AgNO_3$ solution. (e) TEM image of gold NRs synthesized with 0.8 mL of seed solution and 30 mL of 4 mM $AgNO_3$ solution. The amounts of added HCl (12.1 M) are 2.1 mL for NRs shown in a–c and 4.2 mL for NRs shown in d and e. (f) UV–vis–NIR spectra of gold NRs shown in a (black curve), b (green curve), c (red curve), d (blue curve), and e (magenta curve, collected from D_2O solution of gold NRs), respectively. The orange curve is the UV–vis–NIR spectrum of gold NRs synthesized with 0.8 mL of seed solution, 24 mL of 4 mM $AgNO_3$ solution, and 2.1 mL of HCl (12.1 M). All scale bars represent 100 nm.

and thus a blue-shift of the LSPR peak position (from 824 to 705 nm) (Figure 3h). In addition, dog-bone-shaped NRs, as a result of selective deposition of Au onto NR end facets, can often be achieved in several CTAB–aromatic additive systems by providing excess ascorbic acid in the growth solution, which is consistent with a previous report (Figures S22–S24).[39]

Furthermore, monodisperse gold NRs of even higher aspect ratio (>6.0) can be obtained by lowering the pH of NR growth solutions in CTAB/5-bromosalicylic acid system.[32–34,60] Figure 4 shows the TEM images of gold NRs with aspect ratios between 5.9 and 8.5, and the optimized growth conditions are detailed in Table S4. Specifically, at a given pH, reducing the amount of seed particles usually leads to the amplification of both dimensions (length and width) of gold NRs, and the NR aspect ratio can be further tuned by the amount of $AgNO_3$ added. Moreover, the accessible aspect ratio is largely limited by the pH of the NR growth solution: the lower the pH, the higher the possible aspect ratio, albeit at the price of increasing the level of shape impurities. Therefore, the CTAB/5-bromosalicylic acid combination reduces the necessity of using binary micelle-forming surfactants and extended aging time (~one week) for the growth of high aspect ratio gold NRs[31] and extends the range of NR dimensional tunability under growth solution acidities comparable to those previously reported.[33,60]

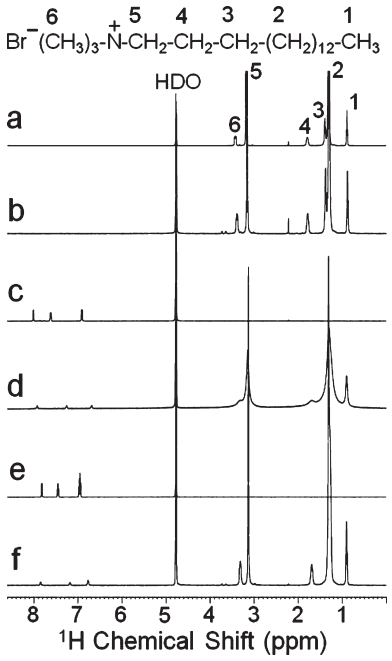

Figure 5. ^{1}H NMR spectra of (a) 10 mM pure CTAB, (b) CTAB-capped gold NRs prepared as previously reported,[31] (c) 2 mM pure 5-bromosalicylic acid, (d) gold NRs synthesized under conditions specified in Table S1 using 5-bromosalicylic acid as the additive, (e) 10 mM pure sodium salicylate, and (f) gold NRs synthesized under conditions specified in Table S1 using sodium salicylate as the additive. All spectra were acquired in D_2O.

Altogether, the results presented in this section demonstrate that the effect of silver ion concentration or the quantity of seed particles is not always to simply change the aspect ratio of gold NR in a linear fashion. The growth behavior of gold NRs in any given CTAB–aromatic additive system is a delicate interplay between elongation and expansion in orthogonal directions from the seed particles, and this kinetically controlled growth process is subject to a variety of factors including reactant concentrations, pH, temperature, and ionic strength. The simultaneous tunability in the optical resonances over a broad spectral range and the control over sample monodispersity of the gold NRs in the CTAB–5-bromosalicylic acid system are very encouraging. We anticipate that further tunability in NR dimensions can be accomplished through finer adjustment of synthetic parameters and also in several other CTAB–aromatic additive combinations.

Numerical calculations such as the FDTD method have been employed to predict the optical extinction cross section and electromagnetic field enhancement in the vicinity of individual metal nanoparticles of various morphologies.[67,68] As shown in Figure S27a, the calculated extinction cross sections of gold NRs of different sizes are in excellent agreement with the experimental extinction spectra (Tables S2 and S4). Indeed, a linear correlation can be established between the LSPR peak position and the average NR aspect ratio determined by TEM studies (Figure S27b). Such a linear dependence has also been predicted theoretically[69] and observed experimentally by several other groups.[31,37,60]

TABLE 1. ^{1}H Chemical Shifts (in ppm) of CTAB, Aromatic Additives, and Gold NRs

CTAB		CTAB-capped gold	CTAB/5-BrSA-capped	CTAB/NaSal-capped
protons[a]	CTAB[b]	NRs	gold NRs	gold NRs
1 (CH_3)	0.89	0.88	0.90	0.90
2 (CH_2)	1.31	1.30	1.31	1.31
3 (CH_2)	1.40	1.38	*c*	*c*
4 (CH_2)	1.79	1.78	1.69	1.69
5 (CH_2)	3.19	3.15	3.15	3.13
6 (CH_2)	3.43	3.38	3.28	3.32

aromatic		CTAB/5-BrSA-capped		CTAB/NaSal-capped
protons[d]	5-BrSA[e]	gold NRs	NaSal[f]	gold NRs
5-H			6.95	6.75
3-H	6.91	6.68	6.98	6.77
4-H	7.61	7.25	7.45	7.18
6-H	8.01	7.92	7.81	7.84

[a] Proton assignments according to previous results from refs 71 and 73. [b] 10 mM CTAB in D_2O. [c] Peaks unresolved due to line broadening. [d] Proton assignments according to previous results from refs 70 and 71. [e] 2 mM 5-BrSA (5-bromosalicylic acid) in D_2O. [f] 10 mM NaSal (sodium salicylate) in D_2O.

NMR and FTIR Studies of Gold Nanorods Synthesized with CTAB–Aromatic Additives. To shed light on the molecular mechanism underlying gold NR growth in CTAB–aromatic additive systems, NMR and FTIR spectroscopies are used to gather more detailed information about the interactions between gold NRs and surfactants. NMR, a powerful technique to study the microstructures and dynamics of surfactants or micellar systems, is employed to examine the surface chemistry of gold NRs. Figure 5 shows the ^{1}H NMR spectra for a D_2O solution of gold NRs synthesized with pure CTAB, CTAB–5-bromosalicylic acid, and CTAB–sodium salicylate, respectively. A summary of ^{1}H chemical shift values is presented in Table 1. The chemical shifts are assigned on the basis of previous reports of NMR spectra of CTAB, sodium salicylate, and related aromatic compounds.[70–73] For CTAB-capped gold NRs, signals from protons (4-H, 5-H, and 6-H) that are close to the quaternary ammonium headgroup are shifted upfield relative to their positions in pure CTAB (Table 1; see Figure 5 for the labeling of CTAB protons), which suggests that CTAB molecules bind to the surface of gold NRs through their headgroups. However, larger upfield shifts from the same CTAB protons are observed for gold NRs involving aromatic additives during synthesis (Table 1). The increased shielding of aliphatic protons near the CTAB headgroup region indicates the presence of aromatic compounds on the gold NR surface and, more importantly, their intercalation between the CTAB headgroups resulting from the synergistic electrostatic and hydrophobic interactions.[70,71] This is further manifested in the aromatic region of the ^{1}H spectra (Figure 6). Table 1 shows

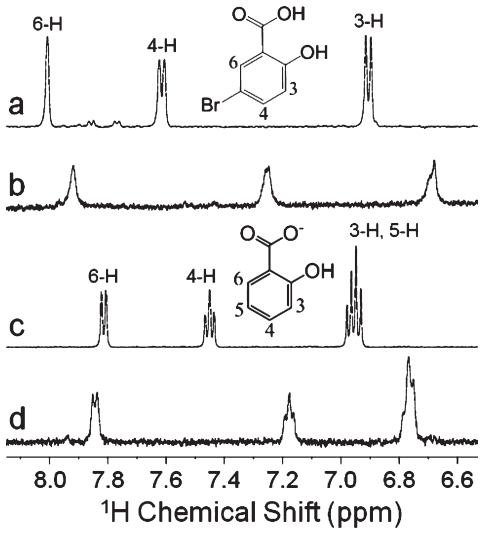

Figure 6. Expanded views of the aromatic region of the ^{1}H NMR spectra shown in (a) Figure 5c, (b) Figure 5d, (c) Figure 5e, and (d) Figure 5f.

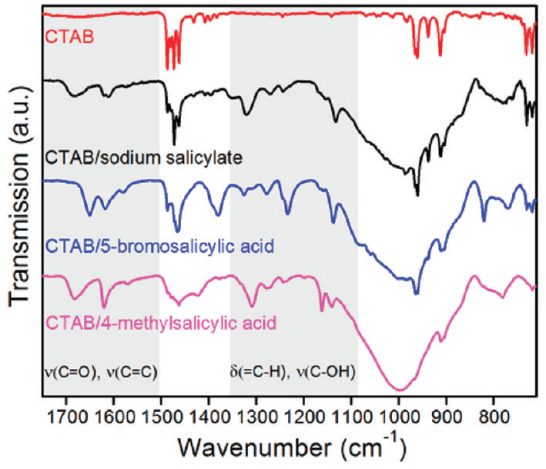

Figure 7. FTIR spectra of gold NRs synthesized under conditions specified in Table S1 using various aromatic additives. The FTIR spectrum of CTAB-capped gold NRs prepared as previously reported[31] without the use of aromatic additives is also presented (red curve).

that signals from all three ring protons of 5-bromosalicylic acid are shifted upfield relative to their peak positions in pure 5-bromosalicylic acid aqueous solution, with the 4-H resonance experiencing the most noticeable shift. A similar trend is observed for salicylate ions present on the gold NR surface. Since the interior is less polar than the surface of CTAB layers, the amount of upfield shifts is also an indication of the average penetration depth of individual aromatic protons into the CTAB layers.[70] These NMR results suggest that the aromatic additives stay embedded within the CTAB capping layers of gold NRs, with the polar substituents (the carboxyl and hydroxyl groups) pointing away from the CTAB hydrocarbon region and thus residing at the surface of CTAB layers. Further evidence supporting this picture includes peak broadening of the aromatic proton resonances consistent with reduced mobility of the benzene rings (Figure 6).

FTIR spectra of gold NRs are also collected as a compliment to NMR studies. The same NR samples for NMR experiments were used for FTIR measurements. As shown in Figure 7, two strong bands are observed in the region 1600−1700 cm^{-1} in the FTIR spectra of gold NRs synthesized using aromatic additives, whereas no identifiable absorption feature appears over the same spectral region for gold NRs made with pure CTAB. On the basis of previous assignments, the higher energy band can be attributed to the C═O stretching of the carboxyl group, and the lower energy band arises from the aromatic ring vibrations.[74−77] Moreover, there are several distinct bands in the region 1050−1350 cm^{-1} for gold NRs synthesized with aromatic additives. Absorptions in this so-called "fingerprint region" contain contributions from in-plane C−H bending, C−O stretching of the hydroxyl group, and vibrations of the benzene ring.[74−77] Since there is usually considerable mixing of vibrational modes in aromatic compounds, a definitive interpretation of these FTIR peaks remain challenging. However, the absence of these complex bands in the FTIR spectrum of gold NRs made with pure CTAB suggests that the aromatic additives are present on the surface of as-synthesized gold NRs, which is consistent with the ^{1}H NMR results.

Insights into the Growth Mechanism of Gold NRs in CTAB−Aromatic Additive Systems. Experimental observations detailed in previous sections have provided important insights into the growth mechanism of gold NRs in CTAB−aromatic additive systems. In this section, we will address several key points relevant to the mechanistic understanding of gold NR formation in CTAB−aromatic additive systems and outline a few questions that need to be addressed by future research.

First, inspired by the literature on the phase behavior and micellar transformations of surfactant−additive mixtures and, in particular, those about cationic surfactant CTAB−aromatic additive systems, we demonstrate in this study that the concentration of CTAB in the gold NR growth solution can be lowered by 50% to 0.05 M compared to the widely used recipes. This is desirable in that it not only reduces the materials costs for gold NR preparation but also offers the added benefit of fewer washing steps that are necessary for NR isolation and purification (Table S5). Moreover, several aromatic additives are proven to be effective in lowering the amount of CTAB needed and, at the same time, in improving dramatically the size and shape uniformity of gold NRs. Importantly, control experiments show that solely reducing the CTAB concentration in the growth solution to ~0.05 M in the absence of any additive leads to deterioration not only in monodispersity but also in the yield of gold NR products, together with a concomitant increase in the level of shape impurities (Figure S28). Moreover, the

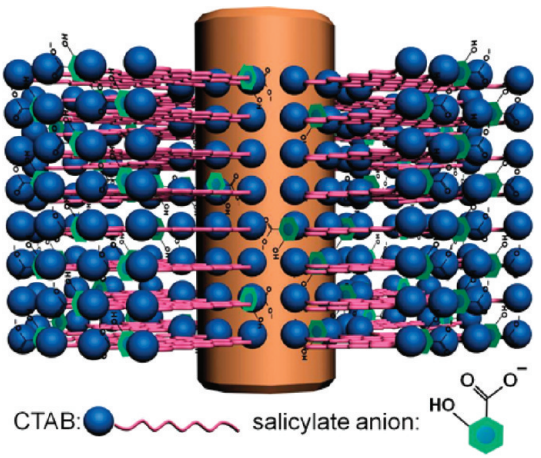

Figure 8. A cartoon illustrating the proposed mechanism to explain the role of aromatic additives (sodium salicylate is shown as an example) in mediating the binding between CTAB bilayers and certain facets of growing gold NRs. Note that surfactant molecules are not drawn at the nanorod tip region for clarity purposes.

reaction becomes more susceptible to impurity ions that might be present in the reagents and thus is hard to reproduce. However, supplying extrinsic bromide ions to the 0.05 M CTAB growth solution by adding potassium bromide salt also promotes gold NR formation (Figure S29).[26,47,48] This observation further confirms the important role of counterions in tuning the interaction/binding between CTAB micelles and developing gold NRs. On the basis of experimental results and, in particular, the NMR and FTIR studies, a binding scheme between CTAB bilayers and gold NRs is proposed and schematically illustrated in Figure 8 using the CTAB–sodium salicylate combination as an example. Furthermore, maintaining a reasonable CTAB concentration (~0.05 M) is necessary for high-quality synthesis of gold NRs, which is supported by poorer sample monodispersity as well as lower yields of NRs in several CTAB–aromatic additive systems when the CTAB concentration is further reduced, even with a concomitantly increased amount of additives (Figures S31, S32). In addition, efforts to scale up the synthesis of gold NRs using the CTAB (0.05 M)–5-bromosalicylic acid combination as an example have proven successful, as evidenced by the NR sample quality (Figure 9 and Figure S7).

Second, the fact that using salicylate-based sodium salts as additives produces shorter NRs compared to aromatic acid additives provides insights into the growth mechanism of gold NRs in CTAB–aromatic additive systems: the salts are readily ionized in water and thus give rise to a higher concentration of anionic counterions compared to those of aromatic acids in the NR growth solutions. While both the acid and salt forms of certain aromatic additives are equally effective in promoting the spherical to rodlike/wormlike micellar transition,[78,79] the salt tends to give less positive micellar surface charges because of electrostatic screening. Therefore, binding between negatively charged Au(III) precursors and positively charged CTAB micelles might be more favorable for the aromatic acid additives, and the NRs formed are longer, as the CTAB layers can "capture" more Au(III) species as the NR grows.

Third, the chemical nature of the aromatic additives is critical for gold NR formation. In contrast to a hydrophilic amino group, bromo, chloro, and methyl groups are hydrophobic and thus do not reduce the tendency of the benzene ring to penetrate into the hydrophobic tail region of the CTAB molecules. This is evidenced by the suppression of NR formation when 5-aminosalicylic acid is employed as the additive (Figures S12, S13), as opposed to the case of 5-bromosalicylic acid or 5-chlorosalicylic acid. For the synthesis of short gold NRs displaying LSPRs less than 700 nm, tunability over the NR aspect ratio can be understood from the fact that the additional methyl group of sodium 3-methylsalicylate can cause a variation in the degree of insertion of the benzene ring into the hydrophobic tail of the CTAB monomer and thus a difference in binding between CTAB micelles and growing gold NRs. On the other hand, variations in NR sample quality mainly in terms of the level of shape impurities among the uses of salicylic acid, 3-methylsalicylic acid, and 4-methylsalicylic acid further demonstrate the delicacy of the CTAB–aromatic additive systems for gold NR synthesis (Figures S6, S9, and S10).

Furthermore, a series of control experiments is carried out to help better understand gold NR growth in CTAB–aromatic additive systems (Table S6 and Figure S33). The aromatic additives employed in this work are phenol derivatives, which are known to be mild reducing agents. Our experimental results show that gold nanostructures do form in an aqueous mixture of aromatic additive and gold chloride (Figures S33a,b,e,f). Although those aromatic additives are sparingly soluble in water, the aromatic additive–CTAB combination can form a homogeneous aqueous solution due to the synergistic condensation of the aromatic molecules onto the palisade layer of CTAB micelles. The reducing power of the additives is apparent on the basis of the observation that the CTAB–additive–$HAuCl_4$ solution becomes colorless after being mixed for about 30 min without ascorbic acid. However, no gold NRs are obtained unless a small amount (~2 mL) of 0.064 M ascorbic acid solution is added to the growth solution (less than the 4.5 mL of ascorbic acid solution required by the standard protocol but still necessary). We speculate that the CTAB–additive–$HAuCl_4$ solution is arrested in a metastable state and the addition of ascorbic acid produces the "active" gold species needed for seed-mediated growth.

Self-Assembly of Gold NRs of Various Aspect Ratios into Ordered Superstructures. Self-organization of monodisperse nanoscale building blocks into ordered arrays represents a facile

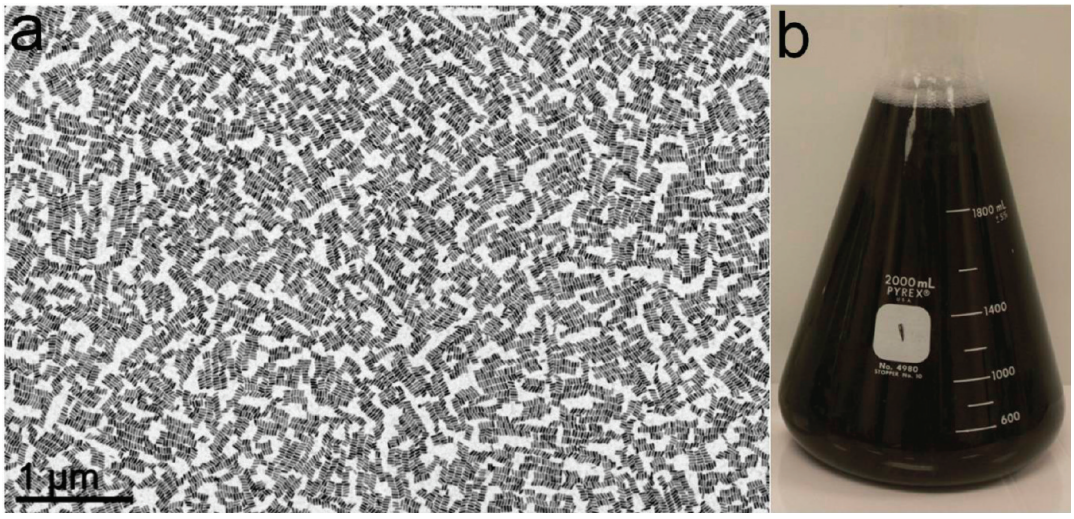

Figure 9. (a) Large-area TEM image of gold NRs obtained by a four-time scale-up synthesis under conditions specified in Table S1 using 5-bromosalicylic acid as the additive. (b) Photograph of the 2000 mL Erlenmeyer flask used for the scale-up synthesis.

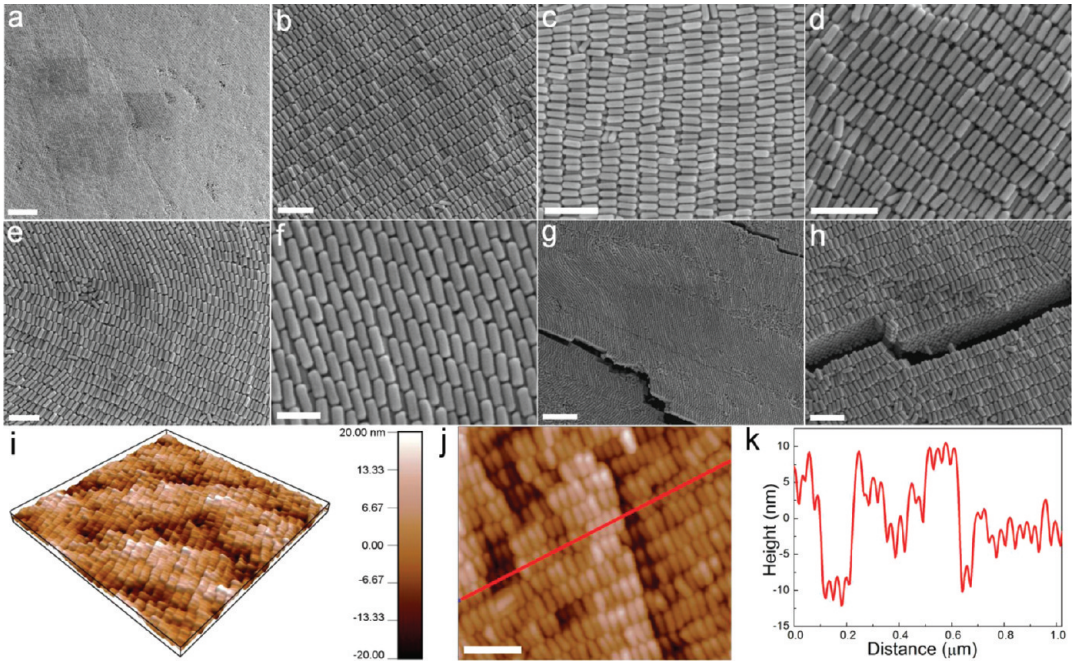

Figure 10. (a–h) SEM images of liquid crystalline assemblies of gold NRs (asepct ratio = 2.9) synthesized under conditions specified in Table S1 using 5-bromosalicylic acid as the additive except with 0.2 mL of seed solution. (i) AFM three-dimensional topography image and (j) AFM height image of gold NR liquid crystalline assemblies. The scan size in (i) is 2 μm × 2 μm. (k) Height analysis of the line profile indicated in (j). Scale bars: (a) 1 μm, (b) 200 nm, (c) 200 nm, (d) 200 nm, (e) 200 nm, (f) 100 nm, (g) 500 nm, (h) 200 nm, (j) 200 nm.

and versatile route for metamaterials with rationally modulated properties.[80,81] In particular, liquid-crystalline-type superstructures or superlattices composed of anisotropic nanocrystals have attracted a fast-growing interest due to the rich phase behaviors resulting from the added complexity of shape anisotropy and the potential for emergent collective properties.[9,82–84] Here we explore the intriguing shape-dependent packing symmetry of ordered NR assemblies by slow evaporation of concentrated gold NR aqueous solutions at room temperature. Onsager's theory on the assembly behavior of hard rodlike colloids shows that above a critical concentration of rods there is a net gain in entropy on transition from isotropic random packing to a nematic liquid crystalline phase.[85] As shown in Figure 10, large-area smectic phases form in dense NR solids, where NRs self-organize into close-packed layers and adjacent layers align nearly parallel into ordered superstructures. AFM studies confirm the three-dimensional nature of gold NR assemblies with a typical domain size of ~10 μm^2 (Figures 10i, S43). AFM height analysis along layers of smectic phases reveals periodic height modulation with a periodicity of 28.0 ± 2.5 nm

(the NR diameter is measured to be 22.0 ± 1.0 nm from TEM images), which is consistent with recent experimental studies showing partially interdigitated CTAB bilayers on the gold NR surface (Figure 10j,k).[86,87] Moreover, the surfaces of gold NR assemblies are not perfectly flat but exhibit height variations corresponding to one or two layers of gold NRs (Figure 10j,k), which could be advantageous for surface-enhanced spectroscopy due to the increased accessibility of local hot-spots.[7−9] However, because of the drying process on a solid substrate (TEM grid in this case), fluctuations in the local NR concentration are expected and the extent of spatial ordering for monodisperse gold NRs is largely limited by the area over which a uniform concentration of NRs can be maintained during the very last stage of deposition. Indeed, this is reflected by the coexistence of smectic and nematic phases on a single TEM grid for gold NRs of various aspect ratios. The nematic phase, characterized by a uniaxial orientational order and lack of positional order, usually forms at less concentrated regions and is more common for NRs of larger aspect ratios (Figures S47−S49). Interestingly, for gold NRs with an aspect ratio less than 4.0, bilayered motifs exhibiting approximately centered-rectangular local packing symmetry are routinely observed (Figures S35, S36, S39, and S45), which has been rarely seen in other NR assemblies.[84] Moreover, the nematic or smectic ordering can be disrupted through continuous bending of neighboring layers, reminiscent of nonequilibrium drying and complex interactions between the NRs (Figure 10e,f). Those wavy gold nanorod assemblies have also been reported by Murphy *et al.* and referred to as "swirling clustering" or "end-to-end cementing".[88] Therefore, theories on the packing of hard rods under equilibrium conditions cannot fully explain the observed structural complexity of gold NR assemblies, and development of a rigorous framework taking into account not only entropic contributions but also nanoscale forces including van der Waals attractions, electrostatic repulsions, dipole−dipole interactions, and, in particular, the role of CTAB layers and counterion interaction in self-assembling gold nanorods is needed.

CONCLUSION

In summary, we have demonstrated that by introducing certain aromatic additives into the well-established seed-mediated synthesis of gold NRs, better control over NR monodispersity and spectral tunability can be achieved using only half the original concentration of CTAB, the cationic micelle-forming surfactant. Uniform gold NRs with LSPRs less than 700 nm are synthesized by adding an appropriate amount of salicylate-based sodium salts to the growth solution. Longer NRs with LSPRs greater than 700 nm are accessible through the use of organic acid additives. Moreover, we show that dimensional control and thus optical tunability of gold NRs can be enhanced with certain CTAB−aromatic additive systems. The results suggest that engineering the interface or interaction between the cationic CTAB micelles and developing gold NRs through rational introduction of small molecules provides exciting new opportunities for size-tunable synthesis of gold NRs as well as other polyhedral-shaped gold nanocrystals. We also demonstrate the formation of three-dimensional complex superstructures self-assembled from monodisperse gold NRs, which are promising substrates for studies on plasmonic coupling[5,89] and enhancement of optical signals including Raman, fluorescence, and upconverted luminescence.[7−9,90]

METHODS

Materials. The following chemicals were purchased and used as received. Hexadecyltrimethylammonium bromide (CTAB, > 98.0%), sodium 3-methylsalicylate (>97.0%), 3-methylsalicylic acid (>98.0%), 4-methylsalicylic acid (>99.0%), 5-bromosalicylic acid (>98.0%), 5-aminosalicylic acid (>98.0%), 5-chlorosalicylic acid (>98.0%), 2,6-dihydroxybenzoic acid (>98.0%), 3,5-dibromosalicylic acid (>98.0%) were purchased from TCI America. Salicylic acid (99+ %) was purchased from Alfa Aesar. Hydrogen tetrachloroaurate trihydrate ($HAuCl_4 \cdot 3H_2O$), sodium salicylate (99%), deuterium oxide (D_2O, 99.8%), and potassium bromide (≥99%) were purchased from Acros Organics. L-Ascorbic acid (BioUltra, ≥99.5%), silver nitrate ($AgNO_3$, >99%), sodium borohydride ($NaBH_4$, 99%), and hydrochloric acid (HCl, 37 wt % in water) were purchased from Sigma Aldrich. Ultrapure water produced with a Milli-Q Integral 5 system was used in all experiments. All glassware was cleaned with aqua regia, rinsed extensively with water, and dried before use.

Synthesis of Gold NRs. The seed solution for gold NRs was prepared as reported previously.[31] A 5 mL amount of 0.5 mM $HAuCl_4$ was mixed with 5 mL of 0.2 M CTAB solution. A 0.6 mL portion of fresh 0.01 M $NaBH_4$ was diluted to 1 mL with water and was then injected into the Au(III)−CTAB solution under vigorous stirring (1200 rpm). The solution color changed from yellow to brownish-yellow, and the stirring was stopped after 2 min. The seed solution was aged at room temperature for 30 min before use.

To prepare the growth solution, 9.0 g of CTAB together with defined amounts of additives (Table S1) were dissolved in 250 mL of warm water (50−70 °C, depending on the additive) in a 500 mL Erlenmeyer flask. The solution was allowed to cool to 30 °C, when a 4 mM $AgNO_3$ solution, as detailed in Table S1, was added. The mixture was kept undisturbed at 30 °C for 15 min, after which 250 mL of 1 mM $HAuCl_4$ solution and, if necessary, a small amount of HCl (37 wt % in water, 12.1 M) was added. After 15 min of slow stirring (400 rpm), 0.064 M ascorbic acid (Table S1) was added, and the solution was vigorously stirred for 30 s until it became colorless. The growth solution had a CTAB concentration of about 0.05 M and was used right after preparation.

Finally, 0.8 mL of seed solution was injected into the growth solution. The resultant mixture was stirred for 30 s and left undisturbed at 30 °C for 12 h for NR growth. The reaction products were isolated by centrifugation at 8500 rpm for 25 min followed by removal of the supernatant. The precipitates were redispersed in 10 mL of water. No size- and/or shape-selective

fractionation was performed except for synthesis that involves adding an extra amount of HCl (results shown in Figure 4). For those samples, one round of purification decreases the amount of shape impurities from ~4% (as-synthesized) to less than 1% of the total number of particles.

Structural and Optical Characterization. Transmission electron microscopy (TEM) images and electron diffraction patterns were acquired on a JEM-1400 microscope operating at 120 kV. High-resolution TEM (HRTEM) images were taken on a JEOL 2010F microscope operating at 200 kV. Scanning electron microscopy (SEM) was performed on a JEOL 7500F HRSEM operating at 2.0 kV. Atomic force microscopy (AFM) images were taken by using a MFP-3D AFM (Asylum Research) operating in the tapping mode. Power X-ray diffraction (XRD) patterns were obtained on the Rigaku Smartlab diffractometer at a scanning rate of 0.1° min^{-1} in the 2θ range from 10° to 90° (Cu Kα radiation, $\lambda = 1.5418$ Å). ^{1}H nuclear magnetic resonance (NMR) spectra were recorded at 300 K on a Bruker DMX 500 MHz NMR spectrometer. The chemical shifts (δ) are expressed in parts per million (ppm) relative to 4,4-dimethyl-4-silapentane-1-sulfonic acid as an internal standard. Prior to NMR acquisition, gold NRs were cleaned by three cycles of centrifugation and redispersion in H_2O (D_2O for the third cycle) to remove excess or unbound CTAB and aromatic additives. Attenuated total reflectance Fourier-transform infrared spectroscopy (ATR-FTIR) was carried out on a Nicolet 6700 (Thermo Fisher) spectrometer using the GATR accessory (Harrick). A 100 μL sample of gold NR aqueous solution (after three rounds of isolation and redispersion in H_2O) was drop-cast onto a glass coverslip that was further dried at 30 °C under vacuum for 24 h. The gold NR film was brought into good contact with the Ge ATR crystal by using a pressure applicator prior to FTIR measurements. Each spectrum was collected at 2 cm^{-1} resolution with 256 scans. Optical extinction spectra were recorded using a Cary 5000 UV/vis/NIR spectrophotometer. pH values of NR growth solutions were measured with an Accument AP72 pH meter (Fisher Scientific).

Finite-Difference Time-Domain (FDTD) Calculations. Numerical simulations for evaluating the extinction spectra were performed using the FDTD method developed by Lumerical FDTD Solutions, Inc. (version 7.5). A multicoefficient fit to the dielectric function of gold was generated in the wavelength range of simulation. In all calculations, the gold NR was modeled as a prolate spheroid with dimensions chosen to match those from electron microscopy studies. The gold NR was enclosed by the simulation volume with perfectly matched layer absorbing boundaries. A three-dimensional nonuniform meshing was used, and a grid size of 0.5 nm was chosen for the inside and immediate vicinity of the gold NR. A total field scattered field source was used to simulate the interaction between a propagating plane wave pulse and the nanorod. The refractive index of the surrounding medium (water) was set as 1.33. The absorption and scattering cross sections for both transverse (not shown since they are much smaller than the longitudinal ones) and longitudinal polarizations were calculated.

Self-Assembly of Gold NRs into Ordered Superstructures. A TEM grid (300 mesh, Electron Microscopy Sciences) was placed at the bottom of a glass vial. A drop (10 μL) of gold NR solution with appropriate concentrations (0.05−0.15 mM) was placed onto the TEM grid. The vial was then partially sealed to allow slow evaporation. The TEM grid was dried after about 6 h.

Conflict of Interest: The authors declare no competing financial interest.

Acknowledgment. We thank J. Gu for assistance with NMR spectroscopy and A. Fafarman for advice on FTIR measurements. X.Y., L.J., H.C., C.Z., N.E., and C.B.M. acknowledge the support from the Office of Naval Research (ONR) Multidisciplinary University Research Initiative (MURI) on Optical Metamaterials through award N00014-10-1-0942. J.C. and V.D.-N. acknowledge the DOE Office of ARPA-E for support under Award DE-AR0000123. G.X. and C.R.K. acknowledge support from the U.S. Department of Energy, Office of Basic Energy Sciences, Division of Materials Science and Engineering, under Award No. DE-SC0002158. Y.K. recognizes support from the Army Research Office (ARO) MURI program under Award No. W911NF-08-1-0364. C.B.M. is also grateful to the Richard Perry University Professorship for support of his supervisor role.

Supporting Information Available: Tables showing the detailed synthetic conditions of gold NRs and pH values of different gold NR growth solutions. Chemical structures of various aromatic additives employed in gold NR synthesis. More TEM images and powder XRD pattern and UV−vis−NIR spectra of gold NRs synthesized under different conditions. Additional SEM and AFM images of liquid crystalline assemblies of gold NRs of different aspect ratios. This material is available free of charge *via* the Internet at http://pubs.acs.org.

REFERENCES AND NOTES

1. Ozbay, E. Plasmonics: Merging Photonics and Electronics at Nanoscale Dimensions. *Science* **2006**, *311*, 189–193.
2. Engheta, N. Circuits with Light at Nanoscales: Optical Nanocircuits Inspired by Metamaterials. *Science* **2007**, *317*, 1698–1702.
3. Jain, P. K.; Huang, X. H.; El-Sayed, I. H.; El-Sayed, M. A. Noble Metals on the Nanoscale: Optical and Photothermal Properties and Some Applications in Imaging, Sensing, Biology, and Medicine. *Acc. Chem. Res.* **2008**, *41*, 1578–1586.
4. Atwater, H. A.; Polman, A. Plasmonics for Improved Photovoltaic Devices. *Nat. Mater.* **2010**, *9*, 205–213.
5. Halas, N. J.; Lal, S.; Chang, W.-S.; Link, S.; Nordlander, P. Plasmons in Strongly Coupled Metallic Nanostructures. *Chem. Rev.* **2011**, *111*, 3913–3961.
6. Tan, S. J.; Campolongo, M. J.; Luo, D.; Cheng, W. L. Building Plasmonic Nanostructures with DNA. *Nat. Nanotechnol.* **2011**, *6*, 268–276.
7. Tao, A.; Kim, F.; Hess, C.; Goldberger, J.; He, R. R.; Sun, Y. G.; Xia, Y. N.; Yang, P. D. Langmuir-Blodgett Silver Nanowire Monolayers for Molecular Sensing Using Surface-Enhanced Raman Spectroscopy. *Nano Lett.* **2003**, *3*, 1229–1233.
8. Lal, S.; Grady, N. K.; Kundu, J.; Levin, C. S.; Lassiter, J. B.; Halas, N. J. Tailoring Plasmonic Substrates for Surface Enhanced Spectroscopies. *Chem. Soc. Rev.* **2008**, *37*, 898–911.
9. Alvarez-Puebla, R. A.; Agarwal, A.; Manna, P.; Khanal, B. P.; Aldeanueva-Potel, P.; Carbo-Argibay, E.; Pazos-Perez, N.; Vigderman, L.; Zubarev, E. R.; Kotov, N. A.; *et al*. Gold Nanorods 3D-Supercrystals as Surface Enhanced Raman Scattering Spectroscopy Substrates for the Rapid Detection of Scrambled Prions. *Proc. Natl. Acad. Sci. U. S. A.* **2011**, *108*, 8157–8161.
10. Lee, A.; Andrade, G. F. S.; Ahmed, A.; Souza, M. L.; Coombs, N.; Tumarkin, E.; Liu, K.; Gordon, R.; Brolo, A. G.; Kumacheva, E. Probing Dynamic Generation of Hot-Spots in Self-Assembled Chains of Gold Nanorods by Surface-Enhanced Raman Scattering. *J. Am. Chem. Soc.* **2011**, *133*, 7563–7570.
11. Kabashin, A. V.; Evans, P.; Pastkovsky, S.; Hendren, W.; Wurtz, G. A.; Atkinson, R.; Pollard, R.; Podolskiy, V. A.; Zayats, A. V. Plasmonic Nanorod Metamaterials for Biosensing. *Nat. Mater.* **2009**, *8*, 867–871.
12. Liu, N.; Tang, M. L.; Hentschel, M.; Giessen, H.; Alivisatos, A. P. Nanoantenna-Enhanced Gas Sensing in a Single Tailored Nanofocus. *Nat. Mater.* **2011**, *10*, 631–636.
13. Wang, L. B.; Zhu, Y. Y.; Xu, L. G.; Chen, W.; Kuang, H.; Liu, L. Q.; Agarwal, A.; Xu, C. L.; Kotov, N. A. Side-by-Side and End-to-End Gold Nanorod Assemblies for Environmental Toxin Sensing. *Angew. Chem., Int. Ed.* **2010**, *49*, 5472–5475.
14. Huang, X. H.; El-Sayed, I. H.; Qian, W.; El-Sayed, M. A. Cancer Cell Imaging and Photothermal Therapy in the Near-Infrared Region by Using Gold Nanorods. *J. Am. Chem. Soc.* **2006**, *128*, 2115–2120.
15. Jain, P. K.; El-Sayed, I. H.; El-Sayed, M. A. Au Nanoparticles Target Cancer. *Nano Today* **2007**, *2*, 18–29.
16. Xue, X.; Wang, F.; Liu, X. Emerging Functional Nanomaterials for Therapeutics. *J. Mater. Chem.* **2011**, *21*, 13107–13127.
17. Wijaya, A.; Schaffer, S. B.; Pallares, I. G.; Hamad-Schifferli, K. Selective Release of Multiple DNA Oligonucleotides from Gold Nanorods. *ACS Nano* **2009**, *3*, 80–86.

18. Grabinski, C.; Schaeublin, N.; Wijaya, A.; D'Couto, H.; Baxamusa, S. H.; Hamad-Schifferli, K.; Hussain, S. M. Effect of Gold Nanorod Surface Chemistry on Cellular Response. *ACS Nano* **2011**, *5*, 2870–2879.
19. Fang, N.; Lee, H.; Sun, C.; Zhang, X. Sub-Diffraction-Limited Optical Imaging with a Silver Superlens. *Science* **2005**, *308*, 534–537.
20. Noginov, M. A.; Zhu, G.; Belgrave, A. M.; Bakker, R.; Shalaev, V. M.; Narimanov, E. E.; Stout, S.; Herz, E.; Suteewong, T.; Wiesner, U. Demonstration of a Spaser-Based Nanolaser. *Nature* **2009**, *460*, 1110–1112.
21. Zijlstra, P.; Chon, J. W. M.; Gu, M. Five-Dimensional Optical Recording Mediated by Surface Plasmons in Gold Nanorods. *Nature* **2009**, *459*, 410–413.
22. Sonnichsen, C.; Reinhard, B. M.; Liphardt, J.; Alivisatos, A. P. A Molecular Ruler Based on Plasmon Coupling of Single Gold and Silver Nanoparticles. *Nat. Biotechnol.* **2005**, *23*, 741–745.
23. Murphy, C. J.; Sau, T. K.; Gole, A. M.; Orendorff, C. J.; Gao, J. X.; Gou, L.; Hunyadi, S. E.; Li, T. Anisotropic Metal Nanoparticles: Synthesis, Assembly, and Optical Applications. *J. Phys. Chem. B* **2005**, *109*, 13857–13870.
24. Jones, M. R.; Osberg, K. D.; Macfarlane, R. J.; Langille, M. R.; Mirkin, C. A. Templated Techniques for the Synthesis and Assembly of Plasmonic Nanostructures. *Chem. Rev.* **2011**, *111*, 3736–3827.
25. Rycenga, M.; Cobley, C. M.; Zeng, J.; Li, W.; Moran, C. H.; Zhang, Q.; Qin, D.; Xia, Y. Controlling the Synthesis and Assembly of Silver Nanostructures for Plasmonic Applications. *Chem. Rev.* **2011**, *111*, 3669–3712.
26. Perez-Juste, J.; Pastoriza-Santos, I.; Liz-Marzan, L. M.; Mulvaney, P. Gold Nanorods: Synthesis, Characterization and Applications. *Coord. Chem. Rev.* **2005**, *249*, 1870–1901.
27. Murphy, C. J.; Thompson, L. B.; Chernak, D. J.; Yang, J. A.; Sivapalan, S. T.; Boulos, S. P.; Huang, J. Y.; Alkilany, A. M.; Sisco, P. N. Gold Nanorod Crystal Growth: From Seed-Mediated Synthesis to Nanoscale Sculpting. *Curr. Opin. Colloid Interface Sci.* **2011**, *16*, 128–134.
28. Sharma, V.; Park, K.; Srinivasarao, M. Colloidal Dispersion of Gold Nanorods: Historical Background, Optical Properties, Seed-Mediated Synthesis, Shape Separation and Self-Assembly. *Mater. Sci. Eng., R* **2009**, *65*, 1–38.
29. Jana, N. R.; Gearheart, L.; Murphy, C. J. Wet Chemical Synthesis of High Aspect Ratio Cylindrical Gold Nanorods. *J. Phys. Chem. B* **2001**, *105*, 4065–4067.
30. Jana, N. R.; Gearheart, L.; Murphy, C. J. Seed-Mediated Growth Approach for Shape-Controlled Synthesis of Spheroidal and Rod-Like Gold Nanoparticles Using a Surfactant Template. *Adv. Mater.* **2001**, *13*, 1389–1393.
31. Nikoobakht, B.; El-Sayed, M. A. Preparation and Growth Mechanism of Gold Nanorods (NRs) Using Seed-Mediated Growth Method. *Chem. Mater.* **2003**, *15*, 1957–1962.
32. Busbee, B. D.; Obare, S. O.; Murphy, C. J. An Improved Synthesis of High-Aspect-Ratio Gold Nanorods. *Adv. Mater.* **2003**, *15*, 414–416.
33. Zhu, J.; Yong, K.-T.; Roy, I.; Hu, R.; Ding, H.; Zhao, L.; Swihart, M. T.; He, G. S.; Cui, Y.; Prasad, P. N. Additive Controlled Synthesis of Gold Nanorods (GNRs) for Two-Photon Luminescence Imaging of Cancer Cells. *Nanotechnology* **2010**, *21*, 285106.
34. Kim, F.; Sohn, K.; Wu, J.; Huang, J. Chemical Synthesis of Gold Nanowires in Acidic Solutions. *J. Am. Chem. Soc.* **2008**, *130*, 14442–14443.
35. Gole, A.; Murphy, C. J. Seed-Mediated Synthesis of Gold Nanorods: Role of the Size and Nature of the Seed. *Chem. Mater.* **2004**, *16*, 3633–3640.
36. Liu, M. Z.; Guyot-Sionnest, P. Mechanism of Silver(I)-Assisted Growth of Gold Nanorods and Bipyramids. *J. Phys. Chem. B* **2005**, *109*, 22192–22200.
37. Perez-Juste, J.; Liz-Marzan, L. M.; Carnie, S.; Chan, D. Y. C.; Mulvaney, P. Electric-Field-Directed Growth of Gold Nanorods in Aqueous Surfactant Solutions. *Adv. Func. Mater.* **2004**, *14*, 571–579.
38. Sau, T. K.; Murphy, C. J. Seeded High Yield Synthesis of Short Au Nanorods in Aqueous Solution. *Langmuir* **2004**, *20*, 6414–6420.
39. Gou, L. F.; Murphy, C. J. Fine-Tuning the Shape of Gold Nanorods. *Chem. Mater.* **2005**, *17*, 3668–3672.
40. Kou, X. S.; Zhang, S. Z.; Tsung, C. K.; Yang, Z.; Yeung, M. H.; Stucky, G. D.; Sun, L. D.; Wang, J. F.; Yan, C. H. One-Step Synthesis of Large-Aspect-Ratio Single-Crystalline Gold Nanorods by Using CTPAB and CTBAB Surfactants. *Chem.—Eur. J.* **2007**, *13*, 2929–2936.
41. Guerrero-Martinez, A.; Perez-Juste, J.; Carbo-Argibay, E.; Tardajos, G.; Liz-Marzan, L. M. Gemini-Surfactant-Directed Self-Assembly of Monodisperse Gold Nanorods into Standing Superlattices. *Angew. Chem., Int. Ed.* **2009**, *48*, 9484–9488.
42. Grzelczak, M.; Sanchez-Iglesias, A.; Rodriguez-Gonzalez, B.; Alvarez-Puebla, R.; Perez-Juste, J.; Liz-Marzan, L. M. Influence of Iodide Ions on the Growth of Gold Nanorods: Tuning Tip Curvature and Surface Plasmon Resonance. *Adv. Funct. Mater.* **2008**, *18*, 3780–3786.
43. Smith, D. K.; Korgel, B. A. The Importance of the CTAB Surfactant on the Colloidal Seed-Mediated Synthesis of Gold Nanorods. *Langmuir* **2008**, *24*, 644–649.
44. Smith, D. K.; Miller, N. R.; Korgel, B. A. Iodide in CTAB Prevents Gold Nanorod Formation. *Langmuir* **2009**, *25*, 9518–9524.
45. Rayavarapu, R. G.; Ungureanu, C.; Krystek, P.; van Leeuwen, T. G.; Manohar, S. Iodide Impurities in Hexadecyltrimethyl Ammonium Bromide (CTAB) Products: Lot-Lot Variations and Influence on Gold Nanorod Synthesis. *Langmuir* **2010**, *26*, 5050–5055.
46. Millstone, J. E.; Wei, W.; Jones, M. R.; Yoo, H.; Mirkin, C. A. Iodide Ions Control Seed-Mediated Growth of Anisotropic Gold Nanoparticles. *Nano Lett.* **2008**, *8*, 2526–2529.
47. Sau, T. K.; Murphy, C. J. Role of Ions in the Colloidal Synthesis of Gold Nanowires. *Philos. Mag.* **2007**, *87*, 2143–2158.
48. Garg, N.; Scholl, C.; Mohanty, A.; Jin, R. C. The Role of Bromide Ions in Seeding Growth of Au Nanorods. *Langmuir* **2010**, *26*, 10271–10276.
49. Khanal, B. P.; Zubarev, E. R. Purification of High Aspect Ratio Gold Nanorods: Complete Removal of Platelets. *J. Am. Chem. Soc.* **2008**, *130*, 12634–12635.
50. Sharma, V.; Park, K.; Srinivasarao, M. Shape Separation of Gold Nanorods Using Centrifugation. *Proc. Natl. Acad. Sci. U. S. A.* **2009**, *106*, 4981–4985.
51. Park, K.; Koerner, H.; Vaia, R. A. Depletion-Induced Shape and Size Selection of Gold Nanoparticles. *Nano Lett.* **2010**, *10*, 1433–1439.
52. Israelachvili, J. N.; Mitchell, D. J.; Ninham, B. W. Theory of Self-Assembly of Hydrocarbon Amphiphiles into Micelles and Bilayers. *J. Chem. Soc., Faraday Trans. 2* **1976**, *72*, 1525–1568.
53. Rehage, H.; Hoffmann, H. Viscoelastic Surfactant Solutions: Model Systems for Rheological Research. *Mol. Phys.* **1991**, *74*, 933–973.
54. Lin, Z.; Cai, J. J.; Scriven, L. E.; Davis, H. T. Spherical-to-Wormlike Micelle Transition in CTAB Solutions. *J. Phys. Chem.* **1994**, *98*, 5984–5993.
55. Hassan, P. A.; Yakhmi, J. V. Growth of Cationic Micelles in the Presence of Organic Additives. *Langmuir* **2000**, *16*, 7187–7191.
56. Aswal, V. K.; Goyal, P. S.; Thiyagarajan, P. Small-Angle Neutron-Scattering and Viscosity Studies of CTAB/NaSal Viscoelastic Micellar Solutions. *J. Phys. Chem. B* **1998**, *102*, 2469–2473.
57. Yoo, H.; Sharma, J.; Yeh, H.-C.; Martinez, J. S. Solution-Phase Synthesis of Au Fibers Using Rod-Shaped Micelles as Shape Directing Agents. *Chem. Commun.* **2010**, *46*, 6813–6815.
58. Rodriguez-Fernandez, J.; Perez-Juste, J.; Mulvaney, P.; Liz-Marzan, L. M. Spatially-Directed Oxidation of Gold Nanoparticles by Au(III)-CTAB Complexes. *J. Phys. Chem. B* **2005**, *109*, 14257–14261.
59. Tsung, C. K.; Kou, X. S.; Shi, Q. H.; Zhang, J. P.; Yeung, M. H.; Wang, J. F.; Stucky, G. D. Selective Shortening of Single-Crystalline Gold Nanorods by Mild Oxidation. *J. Am. Chem. Soc.* **2006**, *128*, 5352–5353.

60. Ni, W.; Kou, X.; Yang, Z.; Wang, J. F. Tailoring Longitudinal Surface Plasmon Wavelengths, Scattering and Absorption Cross Sections of Gold Nanorods. *ACS Nano* **2008**, *2*, 677–686.
61. Jana, N. R.; Gearheart, L.; Obare, S. O.; Murphy, C. J. Anisotropic Chemical Reactivity of Gold Spheroids and Nanorods. *Langmuir* **2002**, *18*, 922–927.
62. Zou, R.; Guo, X.; Yang, J.; Li, D.; Peng, F.; Zhang, L.; Wang, H.; Yu, H. Selective Etching of Gold Nanorods by Ferric Chloride at Room Temperature. *CrystEngComm* **2009**, *11*, 2797–2803.
63. Link, S.; Burda, C.; Nikoobakht, B.; El-Sayed, M. A. Laser-Induced Shape Changes of Colloidal Gold Nanorods Using Femtosecond and Nanosecond Laser Pulses. *J. Phys. Chem. B* **2000**, *104*, 6152–6163.
64. Sohn, K.; Kim, F.; Pradel, K. C.; Wu, J.; Peng, Y.; Zhou, F.; Huang, J. Construction of Evolutionary Tree for Morphological Engineering of Nanoparticles. *ACS Nano* **2009**, *3*, 2191–2198.
65. Carbo-Argibay, E.; Rodriguez-Gonzalez, B.; Gomez-Grana, S.; Guerrero-Martinez, A.; Pastoriza-Santos, I.; Perez-Juste, J.; Liz-Marzan, L. M. The Crystalline Structure of Gold Nanorods Revisited: Evidence for Higher-Index Lateral Facets. *Angew. Chem., Int. Ed.* **2010**, *49*, 9397–9400.
66. Katz-Boon, H.; Rossouw, C. J.; Weyland, M.; Funston, A. M.; Mulvaney, P.; Etheridge, J. Three-Dimensional Morphology and Crystallography of Gold Nanorods. *Nano Lett.* **2011**, *11*, 273–278.
67. Oubre, C.; Nordlander, P. Optical Properties of Metallodielectric Nanostructures Calculated Using the Finite Difference Time Domain Method. *J. Phys. Chem. B* **2004**, *108*, 17740–17747.
68. Myroshnychenko, V.; Rodriguez-Fernandez, J.; Pastoriza-Santos, I.; Funston, A. M.; Novo, C.; Mulvaney, P.; Liz-Marzan, L. M.; de Abajo, F. J. G. Modelling the Optical Response of Gold Nanoparticles. *Chem. Soc. Rev.* **2008**, *37*, 1792–1805.
69. Jain, P. K.; Lee, K. S.; El-Sayed, I. H.; El-Sayed, M. A. Calculated Absorption and Scattering Properties of Gold Nanoparticles of Different Size, Shape, and Composition: Applications in Biological Imaging and Biomedicine. *J. Phys. Chem. B* **2006**, *110*, 7238–7248.
70. Kreke, P. J.; Magid, L. J.; Gee, J. C. ^{1}H and ^{13}C NMR Studies of Mixed Counterion, Cetyltrimethylammonium Bromide/Cetyltrimethylammonium Dichlorobenzoate, Surfactant Solutions: The Intercalation of Aromatic Counterions. *Langmuir* **1996**, *12*, 699–705.
71. Kabir-ud-Din; Kumar, S.; Sharma, D. Role of the Functional Group Position in Producing Viscoelasticity in Micellar Solutions: A ^{1}H NMR study. *J. Surfact. Deterg.* **2002**, *5*, 131–134.
72. Hubert, F.; Testard, F.; Spalla, O. Cetyltrimethylammonium Bromide Silver Bromide Complex as the Capping Agent of Gold Nanorods. *Langmuir* **2008**, *24*, 9219–9222.
73. Orendorff, C. J.; Alam, T. M.; Sasaki, D. Y.; Bunker, B. C.; Voigt, J. A. Phospholipid-Gold Nanorod Composites. *ACS Nano* **2009**, *3*, 971–983.
74. Alvarez-Ros, M. C.; Sanchez-Cortes, S.; Garcia-Ramos, J. V. Vibrational Study of the Salicylate Interaction with Metallic Ions and Surfaces. *Spectrochim. Acta A* **2000**, *56*, 2471–2477.
75. Philip, D.; John, A.; Panicker, C. Y.; Varghese, H. T. FT-Raman, FT-IR and Surface Enhanced Raman Scattering Spectra of Sodium Salicylate. *Spectrochim. Acta A* **2001**, *57*, 1561–1566.
76. Batista, E. A.; Temperini, M. L. A. An *in-situ* SERS and FTIRAS Study of Salicylate Interaction with Copper Electrode. *J Solid State Electrochem.* **2007**, *11*, 1559–1565.
77. Karabacak, M.; Kurt, M. The Spectroscopic (FT-IR and FT-Raman) and Theoretical Studies of 5-bromo-salicylic Acid. *J. Mol. Struct.* **2009**, *919*, 215–222.
78. Manohar, C.; Rao, U. R. K.; Valaulikar, B. S.; Iyer, R. M. On the Origin of Viscoelasticity in Micellar Solutions of Cetyltrimethylammonium Bromide and Sodium Salicylate. *J. Chem. Soc., Chem. Commun.* **1986**, 379–381.
79. Shikata, T.; Hirata, H.; Kotaka, T. Micelle Formation of Detergent Molecules in Aqueous Media. 3. Viscoelastic Properties of Aqueous Cetyltrimethylammonium Bromide Salicylic Acid Solutions. *Langmuir* **1989**, *5*, 398–405.
80. Nie, Z.; Petukhova, A.; Kumacheva, E. Properties and Emerging Applications of Self-Assembled Structures Made from Inorganic Nanoparticles. *Nat. Nanotechnol.* **2010**, *5*, 15–25.
81. Nie, Z. H.; Fava, D.; Kumacheva, E.; Zou, S.; Walker, G. C.; Rubinstein, M. Self-Assembly of Metal-Polymer Analogues of Amphiphilic Triblock Copolymers. *Nat. Mater.* **2007**, *6*, 609–614.
82. Glotzer, S. C.; Solomon, M. J. Anisotropy of Building Blocks and Their Assembly into Complex Structures. *Nat. Mater.* **2007**, *6*, 557–562.
83. Tao, A.; Sinsermsuksakul, P.; Yang, P. Tunable Plasmonic Lattices of Silver Nanocrystals. *Nat. Nanotechnol.* **2007**, *2*, 435–440.
84. Ye, X.; Collins, J. E.; Kang, Y.; Chen, J.; Chen, D. T. N.; Yodh, A. G.; Murray, C. B. Morphologically Controlled Synthesis of Colloidal Upconversion Nanophosphors and Their Shape-Directed Self-Assembly. *Proc. Natl. Acad. Sci. U. S. A.* **2010**, *107*, 22430–22435.
85. Onsager, L. The Effects of Shape on the Interaction of Colloidal Particles. *Ann. N.Y. Acad. Sci.* **1949**, *51*, 627–659.
86. Lee, S.; Anderson, L. J. E.; Payne, C. M.; Hafner, J. H. Structural Transition in the Surfactant Layer that Surrounds Gold Nanorods as Observed by Analytical Surface-Enhanced Raman Spectroscopy. *Langmuir* **2011**, *27*, 14748–14756.
87. Gomez-Grana, S.; Hubert, F.; Testard, F.; Guerrero-Martinez, A.; Grillo, I.; Liz-Marzan, L. M.; Spalla, O. Surfactant (Bi)Layers on Gold Nanorods. *Langmuir* **2012**, *28*, 1453–1459.
88. Sau, T. K.; Murphy, C. J. Self-Assembly Patterns Formed upon Solvent Evaporation of Aqueous Cetyltrimethylammonium Bromide-Coated Gold Nanoparticles of Various Shapes. *Langmuir* **2005**, *21*, 2923–2929.
89. Funston, A. M.; Novo, C.; Davis, T. J.; Mulvaney, P. Plasmon Coupling of Gold Nanorods at Short Distances and in Different Geometries. *Nano Lett.* **2009**, *9*, 1651–1658.
90. Zhang, H.; Li, Y.; Ivanov, I. A.; Qu, Y.; Huang, Y.; Duan, X. Plasmonic Modulation of the Upconversion Fluorescence in $NaYF_4$:Yb/Tm Hexaplate Nanocrystals Using Gold Nanoparticles or Nanoshells. *Angew. Chem., Int. Ed.* **2010**, *49*, 2865–2868.